Virology 381 (2008) 168–177

Contents lists available at ScienceDirect

Virology

journal homepage: www.elsevier.com/locate/yviro

Functional analysis and quantitative determination of the expression profile of human parvovirus B19

Francesca Bonvicini, Claudia Filippone [1], Elisabetta Manaresi, Marialuisa Zerbini, Monica Musiani, Giorgio Gallinella *

Department of Clinical and Experimental Medicine, Division of Microbiology, University of Bologna, Via Massarenti, 9I-40138 Bologna, Italy

ARTICLE INFO

Article history:
Received 24 April 2008
Returned to author for revision 28 July 2008
Accepted 5 September 2008
Available online 5 October 2008

Keywords:
Parvovirus B19
Genome replication
Genome expression
PCR array
Quantitative PCR
Quantitative RT-PCR

ABSTRACT

Comprehension of the pathogenetic potential of human parvovirus B19 requires the definition of the complete spectrum of cellular tropism and a functional analysis of the viral genome in infected cells. In this study, we carried out a systematic functional analysis of B19 virus genome in the course of infection of susceptible bone marrow mononuclear cells and myeloblastoid UT7/EpoS1 cells, in terms of dynamics of nucleic acid synthesis. A PCR array was designed and a comprehensive analysis was performed by quantitative PCR and RT-PCR, yielding extended information on the presence and abundance of the diverse classes of viral nucleic acids, on the temporal regulation of genome expression and on its relationship with the cell cycle. The analysis performed indicate that the synthesis of viral nucleic acids is correlated to the progression through the S phase of the cell cycle, that an extended pattern of transcriptional activity occurs throughout the course of infection, with a maximal rate of transcription preceding the onset of S-phase dependent replication of the viral genome, and that utilization of transcript processing signals is relatively constant throughout the course of infection. The information obtained led to the definition of a unified model of functional and expression profiling of parvovirus B19 genome.

Introduction

Human Parvovirus B19, member of the *Erythrovirus* genus in the *Parvoviridae* family, is a widespread human pathogenic virus that can be associated with an ample range of pathologies and clinical manifestations (Young and Brown, 2004). Structural features of B19 virus are typical of viruses in the family. One molecule of linear single-stranded DNA of either positive or negative polarity, about 5600 bases in length, is encapsidated in isometric virions, approximately 22 nm in diameter. The viral genome is composed of a unique internal region, containing all the coding sequences, flanked by two repeated inverted terminal regions (Fig. 1). Two major open reading frames (ORF) are present in the viral genome. In the left half of the genome, an ORF (frame 3) codes for the non-structural protein NS; in the right half of the genome, an ORF (frame 1) codes for both viral capsid proteins VP1 and VP2. Two minor ORFs are present (frame 2), overlapping with the major ORFs at the centre and at the right end of the genome, coding respectively for a putative 9 kDa protein and an 11 kDa protein. An additional ORF is present (frame 1), coding for a 7.5 kDa protein.

According to the accepted model of replication of the viral genome (Ozawa et al., 1986), the inverted terminal regions are able to fold into hairpin structures that function as origins of replication by priming the conversion of the single-stranded parental template into a double-stranded replicative intermediate; resolution of the terminal hairpins can then occur, operated by the viral non-structural protein, followed by separation of the single stranded replicative products. Expression of the viral genome is driven by a single promoter and is regulated by co- or post-transcriptional processing of RNA (Ozawa et al., 1987a; Yoto et al., 2006). Initiation of transcription occurs at a single site proximal to the left terminal region; processing of RNA includes two distinct and sequential splicing events, each defined by a single donor and two alternative acceptor sites; termination of transcription and cleavage-polyadenylation occur either at a central position, defined by two alternative sites, or at a distal position, defined by a single terminal site proximal to the right terminal region. The different combinations of events and utilization of processing signals result in the production of the whole set of different viral mRNAs that can be translated into the viral non-structural and structural proteins (Ozawa and Young, 1987).

Comprehension of the pathogenetic potential of B19 virus requires the definition of the complete spectrum of cellular tropism and a functional analysis of the viral genome in infected cells. Viral replication and expression are still incompletely described in terms of dynamics and molecular interactions within the cellular environment. Infection of susceptible target cells typically gives rise to a restrictive pattern of infection. It is assumed that viral replication is restricted at the S phase of the cellular cycle and strongly depends on

* Corresponding author. Fax: +39 051 307397.
E-mail address: giorgio.gallinella@unibo.it (G. Gallinella).
[1] Present address: Department of Virology, Haartman Institute, University of Helsinki, Haartmaninkatu, 3 - FIN-00014 Helsinki, Finland.

0042-6822/$ – see front matter © 2008 Elsevier Inc. All rights reserved.
doi:10.1016/j.virol.2008.09.002

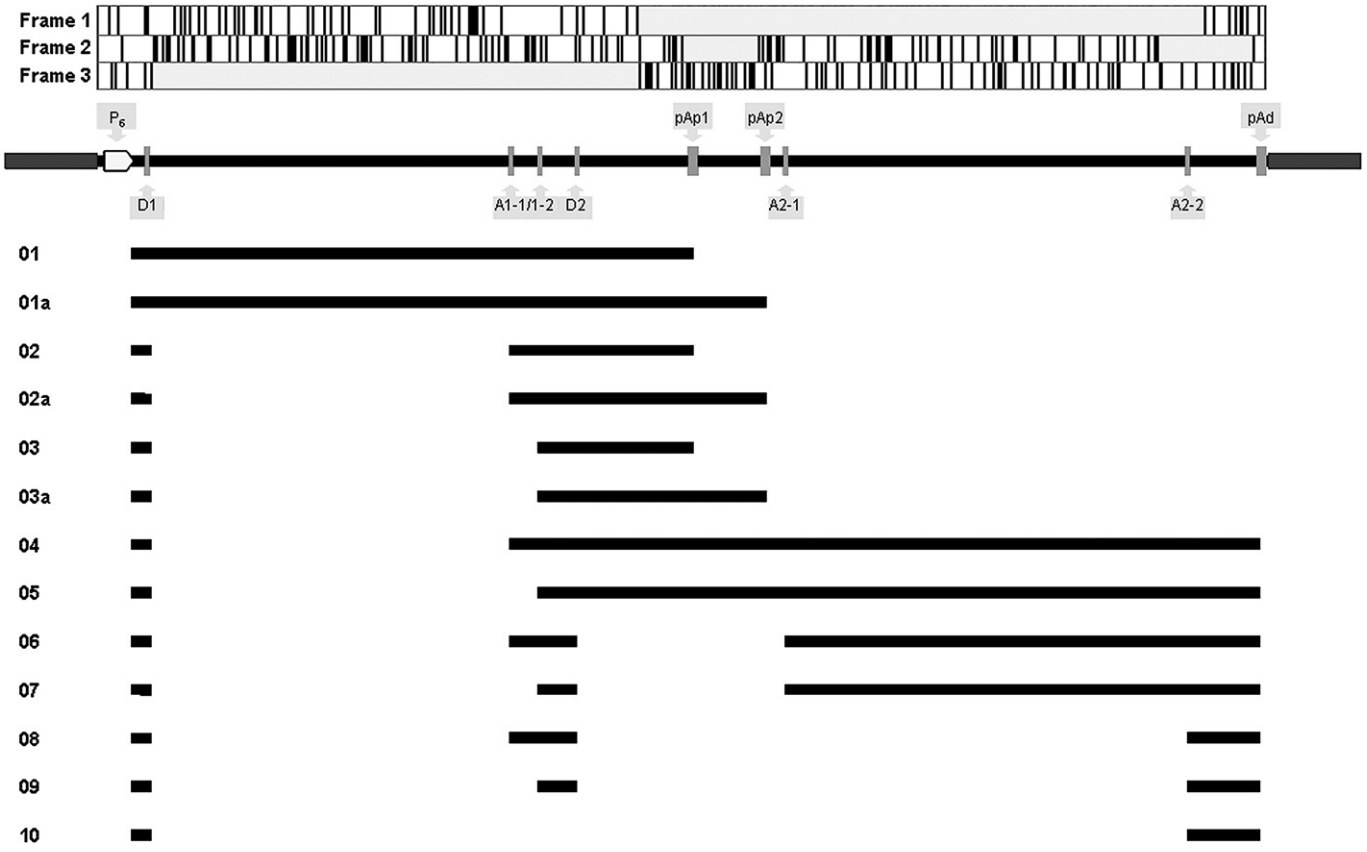

Fig. 1. Outline of parvovirus B19 genome structure and organization. The functional map of B19 virus genome is derived from (Ozawa et al., 1987a; Yoto et al., 2006) and from data obtained in this study.

the presence of cellular permissivity factors, but their identity and relevance still await to be investigated. In erythroid progenitor cells and in some myeloblastoid cell lines, e.g., UT7/Epo and KU812Ep6, the virus can complete a productive replicative cycle (Ozawa et al., 1987b; Shimomura et al., 1992; Miyagawa et al., 1999). In different cell types, such as megakaryoblasts (Srivastava et al., 1990) and other myeloblastoid cell lines (Munshi et al., 1993; Gallinella et al., 2000), the virus may not achieve a productive replicative cycle. Several studies have proposed many diverse mechanisms of regulation (Liu et al., 1991a, 1991b, 1992; Shimomura et al., 1993; Pallier et al., 1997; Brunstein et al., 2000; Gallinella et al., 2000) operating at different stages of the replicative cycle. Quantitative analysis of B19 virus genome replication and expression following in vitro infection experiments indicates that B19 virus genome operates as a single, two-state functional unit (Bonvicini et al., 2006). According to this model, a main restrictive event can be identified in the conversion of the single-stranded parental template into a double-stranded, functionally active template. Then, DNA replication, RNA transcription and co- and post-transcriptional processing of RNA can occur as a unique and coordinated set of events.

In this study, we sought to obtain a systematic functional analysis of B19 virus genome in the course of infection of susceptible bone marrow mononuclear cells and myeloblastoid UT7/EpoS1 cells, in terms of dynamics of nucleic acid synthesis. For this purpose, a PCR array was designed and a comprehensive analysis was performed by quantitative PCR and RT-PCR, yielding extended information on the presence and abundance of the diverse classes of viral nucleic acids. PCR arrays are commonly developed for the analysis of cellular expression profiles, and this study shows that this experimental approach can be effectively applied to a thorough analysis of a viral expression profile. The information obtained led to the definition of a unified model of functional and expression profiling of B19 virus genome.

Results

Design of a PCR array

A systematic functional analysis of B19 virus genome was sought by the design of a PCR array for quantitative PCR and RT-PCR analysis (Table 1), specifically planned to include all the diverse classes of viral nucleic acids (Fig. 2). Oligonucleotide primers were selected on the basis of the known functional map of B19 virus genome, as complementary either to a contiguous sequence, positioned in a defined exon or intron, or to a non-contiguous sequence, corresponding to a defined splice junction. Combinations of primers were optimized in order to discriminate all the different subsets of the viral nucleic acids on the basis of splice definition and exon/intron composition.

The specificity and selectivity of the different primer combinations were tested by amplification of in vitro synthesized DNA and RNA targets, corresponding to the complete internal coding sequence of B19 virus genome, and of DNA and RNA extracted from reference infected and uninfected bone marrow and UT7/EpoS1 cell samples. PCR and RT-PCR products were analyzed by melting profile and by agarose gel electrophoresis, confirming that all amplification reactions exclusively yielded the expected amplification products. The performance of the quantitative PCR and RT-PCR reactions was evaluated on the basis of the analytical characteristics of standard curves obtained. For all primer pairs tested, these yielded a linear range of quantitative evaluation within 10^3–10^8 target copies, with R^2 values constantly >0.99 and average variability in quantitation <6% (0–20%).

Table 1
Primers and primer combinations used in the PCR array for the detection and quantitative evaluation of B19 virus nucleic acids

Primer	Sense	Primer	Antisense	DNA target
R2210	CGCCTGGAACACTGAAACCC	R2355	GAAACTGGTCTGCCAAAGGT	Virus DNA
EC014	TATTTCTCCTGCTACTTGTC	EC184	CCTCGTCATCTTGCTGGTGA	EC01 DNA
Primer	Sense	Primer	Antisense	RNA Target
R0534	TGGGCTGCTTTTTCCTGGAC	R0622	ATAGCTCCATGTTAGTATGT	01/a
		R2101*	CTGGGTGGAGGGCAT*CTGTT*	02/a, 04, 06, 08
		R2221*	CAGTGTTCCAGGCGCC*TGTT*	03/a, 05, 07, 09
R1882	GCGGGAACACTACAACAACT	R2033	GTCCCAGCTTTGTGCATTAC	01/a
R2210	CGCCTGGAACACTGAAACCC	R2355	GAAACTGGTCTGCCAAAGGT	01/a – 09
R2182	GCAGCTTTTTTAACCTCATC	R2377	TCAACCCCAACTAACAGTTC	01/a, 02/a, 04
		R3238*	CAGGGGCAGCTGCAC*AGTTC*	06
		R4897*	GTTTTGCATCTGTAG*AGTTC*	08
R2210	CGCCTGGAACACTGAAACCC	R2377	TCAACCCCAACTAACAGTTC	01/a, 02/a, 03/a, 04, 05
		R3238*	CAGGGGCAGCTGCAC*AGTTC*	06, 07
		R4897*	GTTTTGCATCTGTAG*AGTTC*	08, 09
R2998	CCCGGTACTAACTATGTTGG	R3103	CCAGTTGGCTATACCTAAAG	01a, 02a, 03a, 04, 05
		R3153	CTCTTCATCTGCTACAGTCC	04, 05
R3180	TGGGTTTCAAGCACAAGTAG	R3342	TGCACCAGTGCTGGCTTCTG	04, 05
R3224*	CAGTTTCGTGAACT*GTGCAG*			06, 07
R4883	ATATGACCCCACAGCTACAG	R5014	TGGGCGTTTAGTTACGCATC	06, 07
R4883*	CAGTTTCGTGAACT*CTACAG*			08, 09
R4883**	TGAGCTAACTAACAG*CTACA*			10
R4899	ACACCACAGGCATGGATACG	R5014	TGGGCGTTTAGTTACGCATC	06, 07, 08, 09, 10

Sequence of primers is derived from reference genome sequence NC_000883, as complementary either to a contiguous sequence or to a non-contiguous sequence. In primers marked with *, bases on the 5′ end are complementary to bases on the external side of a splice site, whereas 5–6 bases on the 3′ end (shown in italics) are complementary to bases on the internal side of a splice site. RNA target is defined with respect to the functional map of B19 virus genome.

The developed PCR array was employed in quantitative PCR and RT-PCR in order to obtain a comprehensive quantitative analysis of the expression profile of B19 virus genome in the course of infection of susceptible bone marrow mononuclear cells and myeloblastoid UT7/EpoS1 cells. For each experimental sample, it could be determined the amount of viral DNA, the amount of total viral RNA and, specifically, the relative amount of the different subsets of viral RNA as arising from the differential processing of viral RNA. Quantitation of viral DNA was obtained as an absolute quantitation, by interpolation on standard curves and normalization by the respective quantitation of EC01 DNA as reference target. Quantitation of total viral RNA was similarly obtained as an absolute quantitation, by interpolation on standard curves and normalization by the respective quantitation of EC01 RNA, while quantitation of the different subsets of viral RNA was obtained as a comparative quantitation, normalized to the amount of total viral RNA.

Usage of the first splice donor (D1) and selection of the first splice acceptor (A1-1/2) could be analyzed by combining primer R0534 (common primer positioned in the leader region) with either primer R0622 (specific for unspliced transcripts: 01 and 01a), R2101* (specific for the proximal first acceptor site: 02, 02a, 04, 06, and 08) or R2221* (specific for the distal first acceptor site: 03, 03a, 05, 07, and 09). Unspliced transcripts (01 and 01a) could be selectively amplified by the primer pair R1882–R2033, while the primer pair R2210–R2355, being located in the central exon, could amplify the whole ensemble of viral transcripts and therefore was chosen for the calibrator reaction. Usage of the second splice donor (D2) and selection of the second splice acceptor (A2-1/2) could be analyzed by combining primer R2182 (common primer positioned between sites A1-1 and A1-2) or R2210 (common primer positioned in the central exon) with either primer R2377 (specific for unspliced transcripts: 01, 01a, 02, 02a, 03, 03a, 04, and 05), R3238* (specific for the proximal second acceptor site: 06 and 07) or R4897* (specific for the distal second acceptor site: 08, 09). Comparison among the different sets of primer pairs allowed discrimination of the relative contribution of the products of the first splicing event to the second splicing event. Usage of the proximal acceptor site in the second splicing event could be analyzed by combining primer R3342 with either primer R3180 (specific for

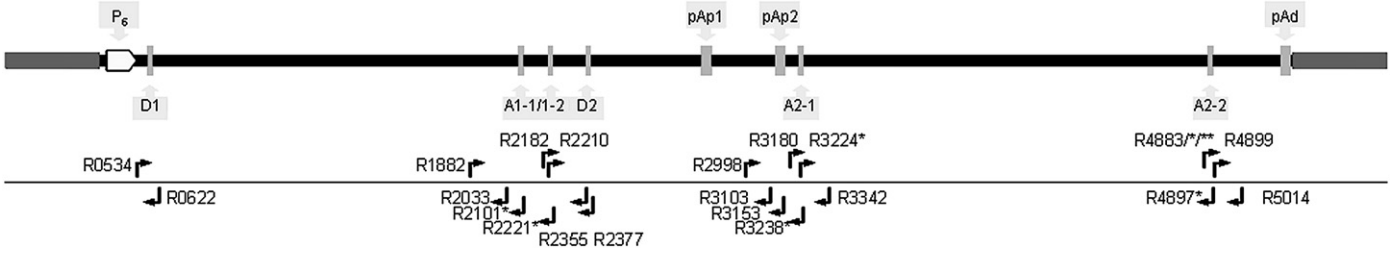

Fig. 2. Position of primers used in the PCR array (see also Table 1) with respect to B19 virus genome. The selectivity of primer pairs in the amplification of specific targets is linked to their distribution with respect to the functional map of B19 virus genome. Sense primer R0534 is positioned upstream of D1 site, antisense primer R0622 is positioned downstream of D1 site, antisense primers R2101* and R2221* are respectively complementary to splice junctions D1/A1-1 and D1/A1-2. Primers R1882 and R2033 are positioned in the region between D1 and A1-1 sites. Sense primer R2182 is positioned between A1-1 and A1-2 sites, and sense primer R2210 is positioned downstream of A1-2 site. Antisense primers R2355 and R2377 are respectively positioned upstream or in correspondence to D2 site. Antisense primers R3238* and R4897* are respectively complementary to splice junctions D2/A2-1 or D2/A2-2. Sense primer R2998 is positioned between pAp1 and pAp2 sites, antisense primer R3103 is positioned upstream and antisense primer R3153 downstream of pAp2 site. Sense primers R3180 and R3224* are respectively positioned upstream of A2-1 site or complementary to D2/A2-1 splice junction, antisense primer R3342 is positioned downstream of A2-1 site. Sense primers R4883, R4883* and R4883** are respectively positioned in correspondence of A2-2 site, or complementary to D2/A2-2 and D1/A2-2 splice junctions. Sense primer R4899 and antisense primer R5014 are positioned in the region between A2-2 and pAd sites.

unspliced transcripts: 01, 01a, 02, 02a, 03, 03a, 04, and 05) or R3224* (specific for the proximal second acceptor site: 06 and 07). Usage of the distal acceptor site in the second splicing event could be analyzed by combining primer R5014 with either primer R4883 (specific for unspliced transcripts: 01, 01a, 02, 02a, 03, 03a, 04, 05, 06, and 07) or R4883* (specific for the distal second acceptor site: 08 and 09). Usage of the proximal and distal cleavage-polyadenylation signals could be analyzed by the primer pairs R2210–R2377 (upstream of pAp1: 01, 01a, 02, 02a, 03, 03a, 04, and 05), R2998–R3103 (upstream of pAp2: 01a, 02a, 03a, 04, and 05), R2998–R3153 (readthrough of pAp: 04 and 05), R4899–R5014 (upstream of pAd: 06, 07, 08, and 09).

The possibility of alternative splicing patterns with respect to the known transcription map of B19 virus genome was also investigated. By using further combinations of primers, it was not possible to detect any unusual splicing of the leader region to the central common exon. When examining the possibility of direct splicing of the leader region to a distal exon, without splicing to the central common exon, it was not possible to detect any splicing of D1 donor to the A2-1 acceptor site, while it was detected a direct splicing of D1 donor to the A2-2 acceptor site. This splicing pattern was confirmed by sequencing of RT-PCR products, and therefore a novel RNA species (transcript 10) was added to the revised transcription map of B19 virus.

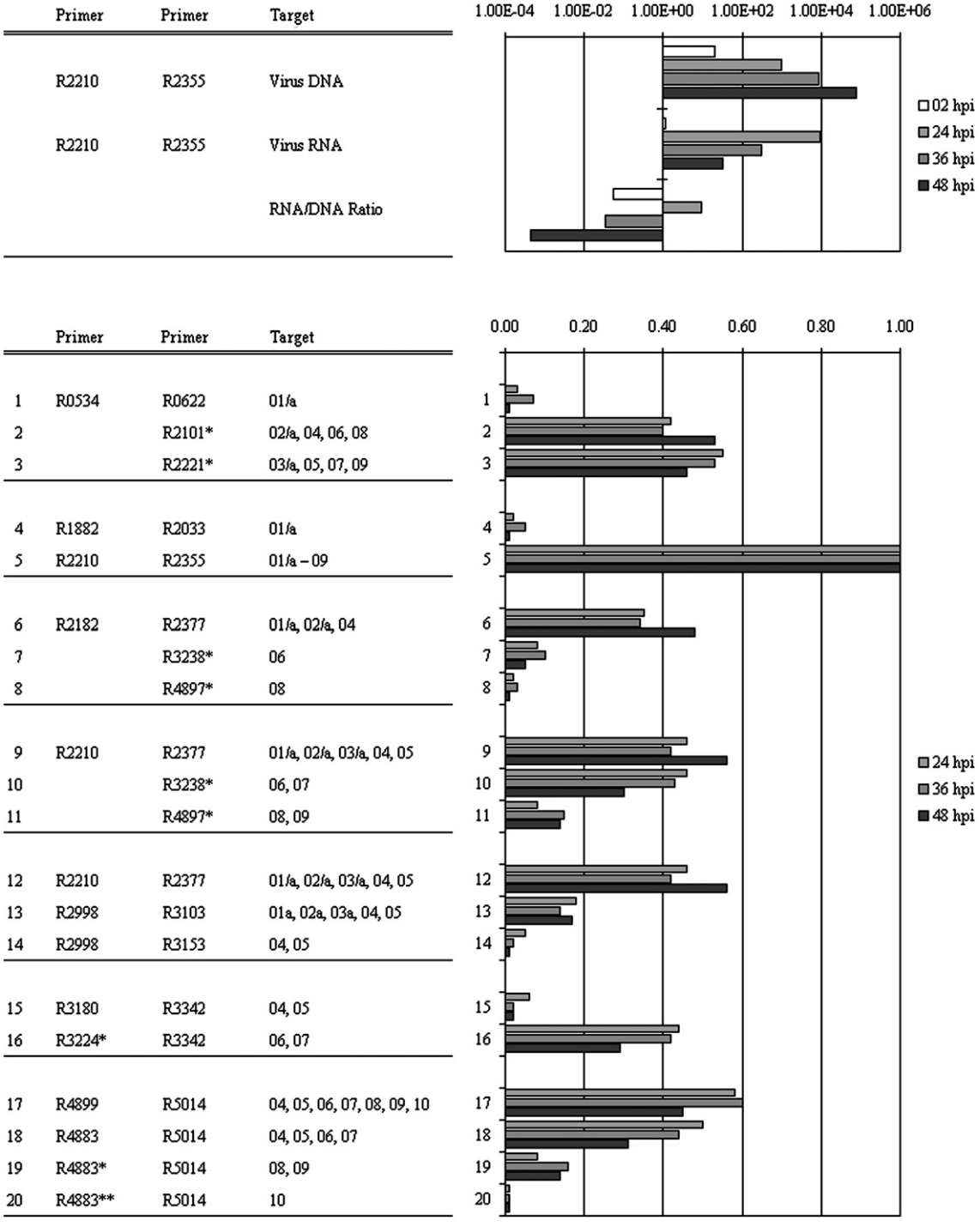

Fig. 3. B19 virus infection of bone marrow mononuclear cells. Amounts of viral DNA and total viral RNA are expressed as relative values per cell; amounts of the different subsets of viral RNA are expressed as fractional values of total viral RNA.

Infection of bone marrow cells

The estimates on the abundance of the diverse classes of viral nucleic acids in the course of infection of bone marrow mononuclear cells are shown in Fig. 3 for a representative experiment. Viral DNA steadily increased from 2 to 24 hpi (+1.7 Log) and from 24 to 48 hpi (+1.9 Log). Viral RNA increased from 2 to 24 hpi (+4.0 Log) and decreased from 24 to 48 hpi (−2.5 Log). Therefore, viral RNA/DNA ratio increased from 2 to 24 hpi (+2.3 Log) and decreased from 24 to 48 hpi (−4.3 Log), indicating an early phase of maximal transcriptional activity compared to replicative activity of viral DNA.

The expression profile of the viral genome was determined on the basis of the relative abundance of the different subsets of viral RNA. Transcriptional activity was already detectable at 2 hpi. At early times in the course of infection, the low amounts of total RNA did not allow to obtain an accurate quantitation of the different RNA species; however, detection of most of the RNA targets indicated the early onset of the full transcriptional programme of B19 virus genome. At later times in the course of infection, from 24 to 48 hpi, the increased amounts of total RNA allowed to determine with higher accuracy the relative abundance of the different RNA species as originated from RNA processing. The data obtained indicated a stable expression profile, as all RNA species were detected throughout the time course of infection and only minor differences were observed in the frequency of utilization of RNA processing signals.

Investigation on the usage of D1 and A1-1/2 splice sites and on the relative abundance of unspliced or spliced RNA species showed an abundance of 1–7% for unspliced RNA (row 1), compared to 93–99% for spliced RNA (rows 2 plus 3), and an equivalent usage of the proximal or distal acceptor sites. Direct comparison of the abundance of unspliced RNA (row 4) relative to the amount of total viral RNA (row 5) yielded a similar estimate.

Investigation on the usage of D2 and A2-1/2 splice sites and on the relative abundance of unspliced/single spliced or double spliced RNA species showed a balanced amount of unspliced/single spliced (row 9) or double spliced RNA (rows 10 plus 11), 42–56% compared to 44–58%. In particular, usage of the proximal acceptor site in the first splicing event led to a high and constant prevalence of single spliced RNA (rows 6 to 8), while usage of the distal acceptor site accounted for most of the double spliced RNA.

For unspliced/single spliced RNA species, cleavage at pAp1 site occurred at a 61–70% frequency (compare rows 12 and 13), leading to an estimate of 14–18% for the abundance of pAp1 readthrough transcripts. Further cleavage at pAp2 site occurred at a 72–94% frequency (compare rows 13 and 14), leading to an estimate of 1–5% for the abundance of pAp2 readthrough transcripts.

For double spliced RNA species, usage of acceptor site A2-1 (row 10) was prevalent over usage of A2-2 (row 11), however decreasing throughout the time course of infection. This led to an abundance of 31–50% of RNA spliced to the proximal second acceptor site and of 8–16% of RNA spliced to the distal second acceptor site. Concordant values were obtained by investigating the relative abundance of contiguous or spliced transcripts to a same distal exon (compare rows 15 and 16 to rows 17 to 19). The RNA arising from direct splicing of the leader sequence to the A2-2 acceptor site was detected only in trace amounts (row 20). The overall amount of RNA cleaved to the pAd site was therefore 45–60% of total viral RNA.

Infection of myeloblastoid cells

Bone marrow mononuclear cells are a heterogeneous population, consisting of different cell types at different stages of differentiation and at different phases of the cell cycle. The myeloblastoid UT7/EpoS1 cells offer the advantage of a more homogeneous population, where also a partial synchronization can be achieved. Infection of UT7/EpoS1 cells as model system was therefore considered suitable for studying any possible relationship between the phase of cell cycle and the replication and expression patterns of B19 virus.

UT7/EpoS1 cells were cultured in minimal medium for 48 h, and then either in the absence (Aph−) or presence (Aph+) of aphidicolin for 16 h. Infection was carried out at the time of release from the cell cycle block, then cell samples were analyzed at different time points post-infection and characterized for both cellular progression through the cell cycle and viral replication and expression. The degree of synchronization achieved was only partial and measurable in terms of variation of distribution of DNA content within the cell population (Fig. 4). The effect of the presence of aphidicolin was evident as a relative depletion of cells in S phase at 0–2 h post-release, followed by a relevant enrichment in cells in S phase at 6 h, while at later times the distribution of cells among the different phases of the cell cycle was relatively unaffected.

The estimates on the abundance of the diverse classes of viral nucleic acids in the course of infection of UT7/EpoS1 cells are shown in Figs. 5 and 6 for a representative experiment. In Aph− cells, the amount of viral DNA was constant between 18 and 24 hpi (−0.1 Log), then increased between 24 and 36 hpi (+1.3 Log) and between 36 and 48 hpi (+0.6 Log). The amount of viral RNA increased between 18 and 24 hpi (+1.3 Log) and between 24 and 36 hpi (+1.3 Log) but not between 36 and 48 hpi (+0.1 Log). Therefore, viral RNA/DNA ratio increased between 18 and 24 hpi (+1.4 Log), was constant between 24 and 36 hpi (0.0 Log) and decreased between 36 and 48 hpi (−0.5 Log). In Aph+ cells, the overall rate of viral nucleic acids synthesis was lower,

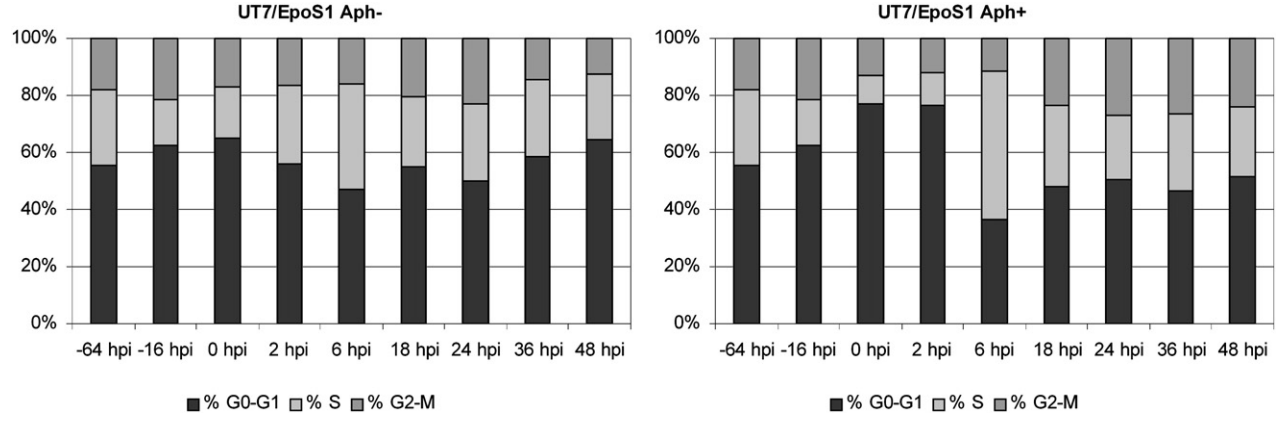

Fig. 4. Distribution of UT7/EpoS1 cells among different phases of the cell cycle as determined by FACS analysis. UT7/EpoS1 cell samples were analyzed before culturing in minimal medium (−64 hpi), after culturing in minimal medium for 48 h (−16 hpi), after culturing either in the absence (Aph−) or presence (Aph+) of aphidicolin for 16 h (0 hpi) and then at different time points (2–48 hpi) in the course of infection.

	Primer	Primer	Target
	R2210	R2355	Virus DNA
	R2210	R2355	Virus RNA
			RNA/DNA Ratio

	Primer	Primer	Target
1	R0534	R0622	01/a
2		R2101*	02/a, 04, 06, 08
3		R2221*	03/a, 05, 07, 09
4	R1882	R2033	01/a
5	R2210	R2355	01/a – 09
6	R2182	R2377	01/a, 02/a, 04
7		R3238*	06
8		R4897*	08
9	R2210	R2377	01/a, 02/a, 03/a, 04, 05
10		R3238*	06, 07
11		R4897*	08, 09
12	R2210	R2377	01/a, 02/a, 03/a, 04, 05
13	R2998	R3103	01a, 02a, 03a, 04, 05
14	R2998	R3153	04, 05
15	R3180	R3342	04, 05
16	R3224*	R3342	06, 07
17	R4899	R5014	04, 05, 06, 07, 08, 09, 10
18	R4883	R5014	04, 05, 06, 07
19	R4883*	R5014	08, 09
20	R4883**	R5014	10

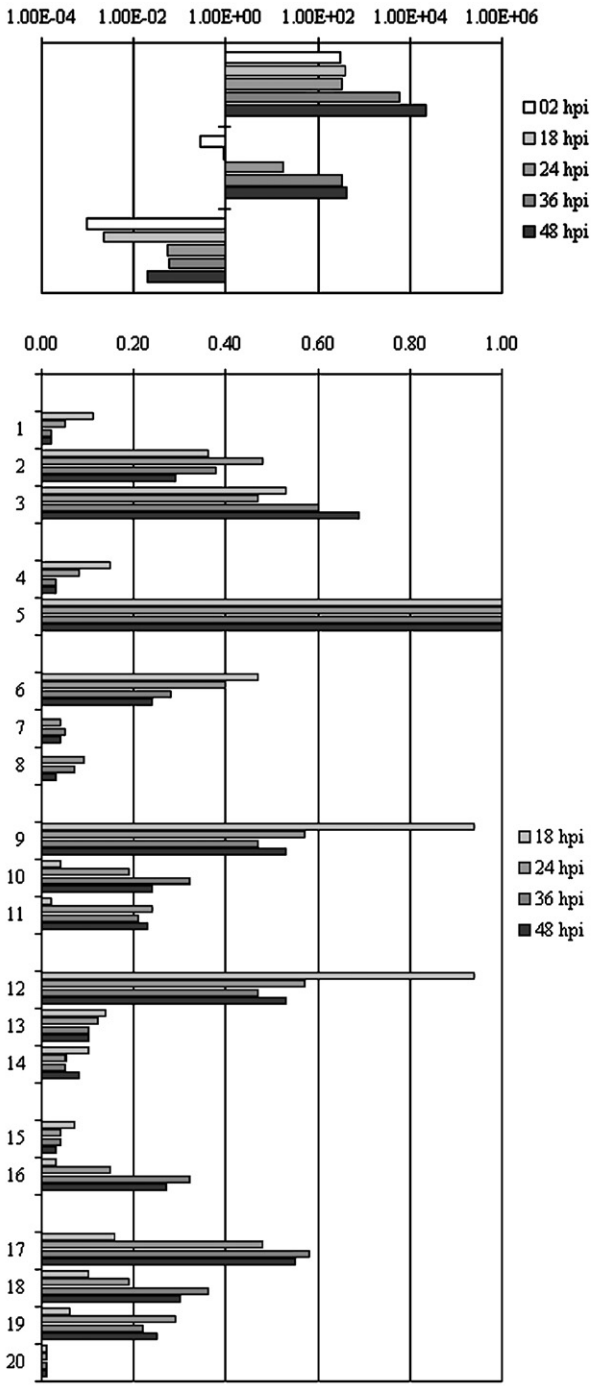

Fig. 5. B19 virus infection of UT7/EpoS1 (Aph−) cells. Amounts of viral DNA and total viral RNA are expressed as relative values per cell; amounts of the different subsets of viral RNA are expressed as fractional values of total viral RNA.

and a sharper temporal distribution of values was observed. Altogether, these data indicate a dependence of viral nucleic acid synthesis on the phase of cell cycle at the start of infection, as a lower fraction of cells in S phase correlates with lower rates of viral nucleic acids synthesis. Then, an early phase of transcriptional activity can occur preceding the onset of the replicative activity of viral DNA, linked to the progression through the cell cycle within the time frame analyzed.

For both Aph− and Aph+ cell populations, transcriptional activity was detected from 6 hpi; however, only at later times in the course of infection, from 18 to 48 hpi, the amount of total RNA allowed to determine the relative abundance of the different RNA species as a result of RNA processing. A distinct expression profile of the viral genome was observed at early (18 hpi) compared to later (24–48 hpi) times in the course of infection.

Investigation on the usage of D1 and A-1/2 splice sites showed a relatively higher abundance of unspliced RNA species at early times post-infection, together with a prevalent usage of the distal compared to the proximal splice acceptor sites. Investigation on the usage of D2 and A2-1/2 splice sites and on the relative abundance of unspliced/single spliced or double spliced RNA species showed a marked shift in the expression pattern. Unspliced/single spliced RNA accounted for almost the totality of viral RNA at 18 hpi, whereas a comparable amount of double spliced RNA was observed at 24–48 hpi. Usage of

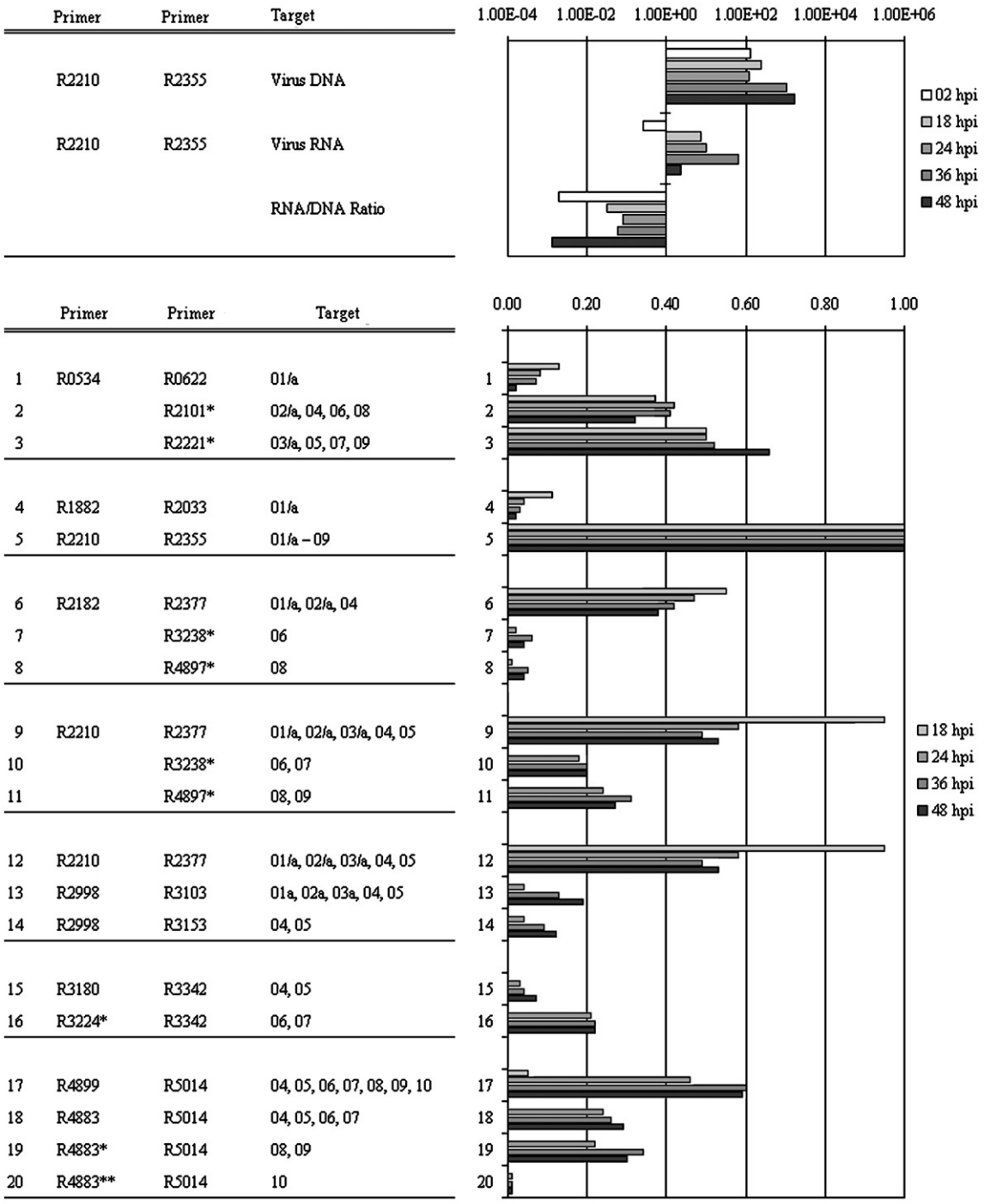

Fig. 6. B19 virus infection of UT7/EpoS1 (Aph+) cells. Amounts of viral DNA and total viral RNA are expressed as relative values per cell; amounts of the different subsets of viral RNA are expressed as fractional values of total viral RNA.

A1-1 acceptor site in the first splicing event was linked to a high and constant prevalence of single spliced RNA, while usage of the A1-2 acceptor site accounted for most of the double spliced RNA. For unspliced/single spliced RNA, cleavage at pAp1 site occurred at a higher frequency at early times, while frequency of cleavage at pAp2 site increased at later times post-infection. For double spliced RNA, usage of the acceptor site A2-1 was comparable to usage of A2-2. This led to a balanced final abundance of RNA spliced to the proximal second acceptor site and of RNA spliced to the distal second acceptor site. Therefore, the overall amount of RNA cleaved to the pAd site increased from minimal levels at early times to high levels at later times in the course of infection.

Discussion

In this study, a systematic functional analysis and definition of the expression profile of B19 virus genome in the course of infection of susceptible bone marrow mononuclear and UT7/EpoS1 cells were obtained by use of a PCR array and quantitative PCR and RT-PCR analysis. In a previous study (Bonvicini et al., 2006), the use of quantitative PCR and RT-PCR for the selective amplification of different regions of the viral genome could only yield information on the relative abundance of expression from different genomic regions. As a further refinement of such experimental approach, the development and application of a PCR array have made it possible to

investigate the presence and abundance of all the diverse classes of viral nucleic acids. This study shows how an experimental approach based on a PCR array can be effectively applied to a comprehensive analysis of a viral expression profile. In our experimental setting, the results obtained led to the definition of a unified model of functional and expression profiling of B19 virus genome.

The compact and complex organization of B19 virus genome poses however a challenging problem. Detection and quantitation of viral DNA and total viral RNA as single targets are straightforward processes, whereas definition of the abundance of the different subsets of viral RNA poses the necessity to obtain a balanced quantitation of multiple targets, all of which are part of a unique ensemble. The fact that all subsets of viral RNA originate from a limited genomic region adds a level of complexity that needs to be solved by designing a redundant PCR array, with different primers positioned on selected regions of the viral genome and different combinations of primers optimized to select specific subsets of targets. In our experimental approach, total RNA would contribute to quantitation of targets at any stage of processing of transcripts, including incompletely processed as well as mature messengers. Hence, our results should be interpreted in terms of definition of frequency of utilization of RNA processing signals. The level of resolution attained by the PCR array could allow to determine the frequency of utilization of each RNA processing signal, and consequently to infer an estimate of the abundance of the different subsets of viral RNA species. However, definite RNA species might not all be distinguishable by this approach: in particular, it will not be possible to discriminate the RNA species differing only on the utilization of pAp1/2 sites.

Several different algorithms for the determination of nucleic acid abundance by means of quantitative PCR and RT-PCR have been proposed (Kubista et al., 2006). In our model system, functional analysis of B19 virus genome throughout the time course of infection requires to obtain quantitation of the abundance of multiple targets within each experimental sample, coupled to a comparison of quantitative values among different samples representative of a time course of infection. Therefore, quantitation of viral nucleic acids was carried out by using two different algorithms. Absolute quantitation by interpolation on standard curves, possible only for contiguous primer pairs, was performed for quantitative evaluation of total viral DNA and RNA and yielded information on viral replication and expression in the course of infection. Comparative quantitation by calibration to total viral RNA, possible for both contiguous and non-contiguous primer pairs, was performed for the definition of a matrix of fractional values for all specific subsets of viral RNA targets and yielded information on the pattern of expression at selected time points in the course of infection. It should always be stressed that our experimental approach yielded information on average values within a heterogeneous cell population, and that quantitative results can only be interpreted in terms of variation of the relative abundance of different nucleic acid species.

Within the limits posed by the experimental setting and the analytical procedure followed, our results yielded extensive information on the temporal regulation of genome expression and its relationship with the cell cycle. The dependence of B19 virus replication on cellular S phase is assumed because of the general biology of the *Parvoviridae* family, but it has not been thoroughly investigated. Although the heterogeneous bone marrow cells do not allow to draw conclusions on the relationship between viral macromolecular synthesis and cellular cycle, observations on UT7/EpoS1 cells partially synchronized by the use of aphidicolin as a DNA polymerase inhibitor, which block cells at early S phase, confirm that viral synthesis are correlated to progression through the S phase of the cell cycle. A first step in macromolecular synthesis of the viral replicative cycle is the conversion of the incoming single-stranded in a double-stranded molecule, in order that the viral genome can start transcriptional and replicative activity (Gallinella et al., 2000; Bonvicini et al., 2006). The analytical performance of quantitative PCR does not allow discrimination between the two forms, nevertheless our data suggest that synthesis of the complementary strand may be critically dependent on the S phase of the cell cycle and can therefore be considered a crucial restrictive event in the viral cycle. Following this step, an extended pattern of transcriptional activity can constantly be present from immediate early times throughout the course of infection, with a maximal rate of transcription preceding the onset of S-phase dependent replication of the viral genome. The reciprocal relationship between B19 virus and cell cycle may however be more complex, as the virus can block the progression through the cell cycle and induce apoptosis (Morita et al., 2001, 2003).

Our study also indicates the presence of differences in genome expression among different cell types. Transcriptional activity depends on *cis*-elements in the single P6 promoter, and on interaction of basic transcriptional machinery with cellular factors and viral NS protein (Raab et al., 2001, 2002). Replicative activity similarly depends on integrity of the terminal hairpins as origins of replication and rely on viral NS protein in addition to cellular machinery (Zhi et al., 2006). Transcriptional activity, as determined by RNA/DNA ratio, appeared to be stronger in bone marrow cells than in UT7/EpoS1 cells, while the difference between cell types was less pronounced in terms of replicative activity of viral DNA.

The presence and utilization of splicing and cleavage-polyadenylation signals determine the relative abundance of the different RNA species originating from a single and compact transcriptional unit. Utilization of the processing signals emerged to be relatively constant throughout the viral infection cycle, with the only relevant exception of the difference observed at early compared to later times post-infection in UT7/EpoS1 cells. In these cells it was observed an overall reduced rate of splicing both of the first and, to a high extent, of the second intron, in the presence of a constant utilization of the pAp1/2 cleavage sites. It might therefore be possible to indicate an early modulation in expression profiling of the viral genome, linked to transition from a low splicing, prevalent pAp cleavage to a high splicing, balanced pAp/pAd cleavage.

A further regulated event appears to be the differential relative utilization of splice acceptors A1-1/2 or A2-1/2, with differences emerging between bone marrow or UT7/EpoS1 cells. For A1-1/2 acceptor sites, a balanced utilization is observed in bone marrow cells compared to a prevalent utilization of A1-2 over A1-1 site in UT7/EpoS1 cells. For A2-1/2 acceptor sites, a prevalent utilization of A2-1 over A2-2 is observed in BM cells compared to a balanced utilization in UT7/EpoS1 cells. Finally, definition of the first splice acceptor seems to influence the frequency of utilization of the second splice donor, and consequently the relative utilization of the proximal or distal cleavage-polyadenylation signals.

The information obtained on viral expression profile should be considered in comparison to what is the current paradigm on B19 virus expression. Earlier data on expression of B19 virus genome, in fact, suggested the presence of distinct early and late expression patterns linked to viral genome replication and that definition of cleavage would be of importance to determine the expression profiling of the viral genome in permissive or non-permissive cell systems (Shimomura et al., 1993). However, any regulation does not seem to be strictly related to replication, as a steady transcription pattern is settled before the onset of a constantly detected genome replication, and it should be stressed that the regulated event appears to be splicing definition more than cleavage signal utilization. Our previous data (Bonvicini et al., 2006) suggested that B19 virus genome should be considered a single replicative and transcriptional unit. The innovative analytical method employed in the present study could add extended information and yield an accurate measurement at the level of the diverse classes of viral nucleic acids. The analysis performed confirm and further refine such single-unit model, demonstrating the presence of a coordinated

set of events involved in DNA replication, RNA transcription and co- and post-transcriptional processing of RNA. The discrepancy emerging between data obtained by our quantitative analysis and previous data reported in the literature can be attributed to differences in the experimental designs and to the high resolution and analytical performance of quantitative PCR and RT-PCR assays. As a note of caution, as the determined amounts of viral nucleic acids are averaged over the entire cell population, our data cannot exclude that different patterns of expression might co-exist within a heterogeneous cell population characterized by different cellular environments.

As a final consideration, the RNA complement is only indicative of the potential viral proteome. In fact, the transcription map has to be reconsidered in view of the presence of a-, mono- or bicistronic mRNAs, and of the effective efficiency of translation of each ORF. In particular, apart from the major ORFs in frame 3, coding for NS protein, and in frame 1 coding for VP1/2 proteins, the minor ORFs potentially coding for low Mr proteins are still to be fully characterized (St Amand et al., 1991; Luo and Astell, 1993). In frame 2, both ORFs in the middle and right end of the genome have similar topographical relation with respect to transcripts, however evidence for translation of the middle ORF in a putative 9 kDa protein is lacking, while translation of the right end ORF gives rise to a 11 kDa protein, essential for viral infectivity. Similarly, evidence of translation of the small ORF positioned in frame 1 ahead of the ORF for VP proteins, coding for 7.5 kDa protein, is incomplete. In the future, a proteomic analysis approach will be required for characterization of the dynamics and interactions of viral proteins produced in infected cells, and of virus-induced cellular alterations.

Materials and methods

Cells

Bone marrow mononuclear cells from normal volunteer donors were obtained as frozen stocks from Cambrex. Cells were cultured in IMDM, 10% FCS, 10 ng/ml IL-3 (Genzyme) and 10 U/ml Epo (NeoRecormon, Roche), at 37 °C and 5% CO_2, at an initial density of 1×10^6 cells/ml. After 2 days, non-adherent cells were recovered and used for the infection experiments.

UT7/EpoS1 cells (a kind gift of K. Sugamura) were cultured in RPMI, 10% FCS and 2 U/ml Epo, at 37 °C and 5% CO_2, at densities between 2×10^5–1×10^6 cells/ml. For synchronization, cells were cultured in RPMI, 20 mM Hepes, 0.5% FCS and 2 U/ml Epo for 48 h, at an initial density of 3×10^5 cells/ml, then either in the presence or absence of 2 μg/ml aphidicolin (Sigma) for 16 h. Cells were then washed, recovered and used for the infection experiments by culturing in complete medium for up to 48 h. Cell populations were analyzed by PI staining (Nusse et al., 1990) and FACS analysis (Bryte HS, by Modfit software, BioRad) for determination of the distribution of cells among different phases of the cell cycle.

Virus and infection

A viremic serum sample, identified in our laboratory in the course of routine diagnostic analysis, was used as source of virus for the infection experiments. The viremic serum contained 10^{12} B19 virus genome equivalents (geq)/ml, as determined by quantitative PCR analysis (Gallinella et al., 2004), and did not contain anti-B19 specific IgM or IgG antibodies detectable by commercial ELISA tests (Biotrin).

For infection, cells were incubated at a density of 10^6 cells/ml in minimal medium in the presence of 10^{-3} volume of viremic serum, in order to obtain a multiplicity of infection (moi) of 10^3 geq/cell. Following adsorption for 2 h at 37 °C, the inoculum virus was washed and the cells were incubated at 37 °C in complete medium at an initial density of 1×10^6 cells/ml. Constant volumes of cell cultures, corresponding to 0.5 ml of the initial cell culture volume, were collected at different time points post-infection (hpi) for nucleic acid purification and analysis. Productive infection was ascertained by immunofluorescence detection of viral NS protein (by a monoclonal human antibody against NS protein, kind gift of S. Modrow) and VP proteins (by a monoclonal mouse antibody against VP1 and VP2 proteins, MAB8293, Chemicon).

Nucleic acid purification

For nucleic acid purification, cell culture samples were processed both by using the MagNA Pure instrument and the MagNA Pure Total Nucleic Acid Isolation Kit (Roche), in order to obtain a total nucleic acid fraction, and by using the ToTally RNA purification kit (Ambion) following the manufacturer's protocol, in order to obtain a nucleic acid fraction enriched in RNA.

PCR analysis

Standards and primers

Standard targets for the amplification reactions were obtained from plasmids pHR0 and pEC01 (Gallinella et al., 2004). Plasmid pHR0 contains an insert corresponding to the full internal region of B19 virus genome (nt. 345–5245). Plasmid pEC01 contains as insert a synthetic sequence, unrelated to other natural sequences present in the NCBI Nucleotide Database. In vitro synthesized DNA and RNA were quantified by spectrophotometric analysis and used as copy number standards in the amplification reactions. In the case of pEC01, in vitro synthesized DNA and RNA were added at 10^9 geq/ml to the sample lysis buffer in the nucleic acid purification procedure and so copurified with sample DNA and RNA as analytical control reagents and as reference targets in the amplification reactions.

PCR primers were specifically designed by using Clone Manager 8.0 software (Scientific & Educational Software), based on sequence NC_000883 in the NCBI Genome Database as reference sequence, and were obtained from MWG Biotech. Name, position, sequence and target specificity of the designed primers are described in Table 1. Oligonucleotide primers were designed on the basis of the known functional map of B19 virus genome, as complementary either to a contiguous sequence, positioned in a defined exon or intron, or to a non-contiguous sequence, corresponding to a defined splice junction. In the non-contiguous primers, marked with *, bases on the 5′ end are complementary to bases on the external side of a splice site, whereas 5–6 bases on the 3′ end (shown in italics) are complementary to bases on the internal side of a splice site.

Amplification reactions

For the analysis of viral DNA, an aliquot of the total nucleic acid fraction, corresponding to 0.05 ml of the cell culture volume, was directly amplified. For the analysis of viral RNA, a corresponding aliquot of the RNA enriched fraction was first treated with Turbo DNAfree reagent (Ambion) and then amplified. Real-time PCR and RT-PCR were carried out by using the RotorGene 3000 system (Corbett Research) and SybrGreen detection of amplification products. Amplification reactions were performed by using QuantiTect PCR SybrGreen PCR Kit (Qiagen) or QuantiTect SybrGreen RT-PCR Kit (Qiagen), including 10 pmol of each specific primer pair. For PCR, thermal profile consisted in 15 min at 95 °C, then 40 cycles of 15 s at 95 °C, 30 s at 50 °C, and 30 s at 70 °C coupled with signal acquisition. For RT-PCR, two parallel reactions were performed for each sample, either including (RT+) or omitting (RT−) the reverse transcriptase from the reaction mix, and performing an initial step consisting in 30 min at 50 °C, before the amplification reaction with a standard thermal profile. A final melting curve was performed, with thermal profile ramping from 50 °C to 95 °C at a 12 °C/min rate, coupled with continuous signal acquisition.

Data analysis

Fluorescence emission was recorded in the FAM/Sybr channel of the instrument and analyzed by using the functions available in the

RotorGene 6.0 software. Melting analysis was used for the determination of the specificity of the amplification products by defining, for each reaction, the melting profile and the Tm of the products; specific accumulation of the amplification products was also confirmed by agarose gel electrophoretic analysis. Quantitation of viral DNA and of total viral RNA was obtained by the absolute quantitation algorithm, relative to standard targets and normalized to the amount of EC01. Quantitation of different subsets of viral RNA was obtained by the comparative quantitation algorithm, calibrated and internally normalized to the amount of total viral RNA.

Acknowledgments

We gratefully acknowledge Dr. Manuela Voltattorni (Interdepartmental Center for Biotechnology, Bologna) for performing FACS analysis. This work was supported by funds from MUR (Ministero dell'Università e della Ricerca) and from the University of Bologna.

Appendix A. Supplementary data

Supplementary data associated with this article can be found, in the online version, at doi:10.1016/j.virol.2008.09.002.

References

Bonvicini, F., Filippone, C., Delbarba, S., Manaresi, E., Zerbini, M., Musiani, M., Gallinella, G., 2006. Parvovirus B19 genome as a single, two-state replicative and transcriptional unit. Virology 347, 447–454.

Brunstein, J., Soderlund-Venermo, M., Hedman, K., 2000. Identification of a novel RNA splicing pattern as a basis of restricted cell tropism of erythrovirus B19. Virology 274, 284–291.

Gallinella, G., Manaresi, E., Zuffi, E., Venturoli, S., Bonsi, L., Bagnara, G.P., Musiani, M., Zerbini, M., 2000. Different patterns of restriction to B19 parvovirus replication in human blast cell lines. Virology 278, 361–367.

Gallinella, G., Bonvicini, F., Filippone, C., Delbarba, S., Manaresi, E., Zerbini, M., Musiani, M., 2004. Calibrated real-time PCR for evaluation of parvovirus b19 viral load. Clin. Chem. 50, 759–762.

Kubista, M., Andrade, J.M., Bengtsson, M., Forootan, A., Jonak, J., Lind, K., Sindelka, R., Sjoback, R., Sjogreen, B., Strombom, L., Stahlberg, A., Zoric, N., 2006. The real-time polymerase chain reaction. Mol. Aspects Med. 27, 95–125.

Liu, J.M., Fujii, H., Green, S.W., Komatsu, N., Young, N.S., Shimada, T., 1991a. Indiscriminate activity from the B19 parvovirus p6 promoter in nonpermissive cells. Virology 182, 361–364.

Liu, J.M., Green, S.W., Hao, Y.S., McDonagh, K.T., Young, N.S., Shimada, T., 1991b. Upstream sequences within the terminal hairpin positively regulate the P6 promoter of B19 parvovirus. Virology 185, 39–47.

Liu, J.M., Green, S.W., Shimada, T., Young, N.S., 1992. A block in full-length transcript maturation in cells nonpermissive for B19 parvovirus. J. Virol. 66, 4686–4692.

Luo, W., Astell, C.R., 1993. A novel protein encoded by small RNAs of parvovirus B19. Virology 195, 448–455.

Miyagawa, E., Yoshida, T., Takahashi, H., Yamaguchi, K., Nagano, T., Kiriyama, Y., Okochi, K., Sato, H., 1999. Infection of the erythroid cell line, KU812Ep6 with human parvovirus B19 and its application to titration of B19 infectivity. J. Virol. Methods 83, 45–54.

Morita, E., Tada, K., Chisaka, H., Asao, H., Sato, H., Yaegashi, N., Sugamura, K., 2001. Human parvovirus B19 induces cell cycle arrest at G(2) phase with accumulation of mitotic cyclins. J. Virol. 75, 7555–7563.

Morita, E., Nakashima, A., Asao, H., Sato, H., Sugamura, K., 2003. Human parvovirus B19 nonstructural protein (NS1) induces cell cycle arrest at G(1) phase. J. Virol. 77, 2915–2921.

Munshi, N.C., Zhou, S., Woody, M.J., Morgan, D.A., Srivastava, A., 1993. Successful replication of parvovirus B19 in the human megakaryocytic leukemia cell line MB-02. J. Virol. 67, 562–566.

Nusse, M., Beisker, W., Hoffmann, C., Tarnok, A., 1990. Flow cytometric analysis of G1- and G2/M-phase subpopulations in mammalian cell nuclei using side scatter and DNA content measurements. Cytometry 11, 813–821.

Ozawa, K., Young, N., 1987. Characterization of capsid and noncapsid proteins of B19 parvovirus propagated in human erythroid bone marrow cell cultures. J. Virol. 61, 2627–2630.

Ozawa, K., Kurtzman, G., Young, N., 1986. Replication of the B19 parvovirus in human bone marrow cell cultures. Science 233, 883–886.

Ozawa, K., Ayub, J., Hao, Y.S., Kurtzman, G., Shimada, T., Young, N., 1987a. Novel transcription map for the B19 (human) pathogenic parvovirus. J. Virol. 61, 2395–2406.

Ozawa, K., Kurtzman, G., Young, N., 1987b. Productive infection by B19 parvovirus of human erythroid bone marrow cells in vitro. Blood 70, 384–391.

Pallier, C., Greco, A., Le Junter, J., Saib, A., Vassias, I., Morinet, F., 1997. The 3′ untranslated region of the B19 parvovirus capsid protein mRNAs inhibits its own mRNA translation in nonpermissive cells. J. Virol. 71, 9482–9489.

Raab, U., Bauer, B., Gigler, A., Beckenlehner, K., Wolf, H., Modrow, S., 2001. Cellular transcription factors that interact with p6 promoter elements of parvovirus B19. J. Gen. Virol. 82, 1473–1480.

Raab, U., Beckenlehner, K., Lowin, T., Niller, H.H., Doyle, S., Modrow, S., 2002. NS1 protein of parvovirus B19 interacts directly with DNA sequences of the p6 promoter and with the cellular transcription factors Sp1/Sp3. Virology 293, 86–93.

Shimomura, S., Komatsu, N., Frickhofen, N., Anderson, S., Kajigaya, S., Young, N.S., 1992. First continuous propagation of B19 parvovirus in a cell line. Blood 79, 18–24.

Shimomura, S., Wong, S., Brown, K.E., Komatsu, N., Kajigaya, S., Young, N.S., 1993. Early and late gene expression in UT-7 cells infected with B19 parvovirus. Virology 194, 149–156.

Srivastava, A., Bruno, E., Briddell, R., Cooper, R., Srivastava, C., van Besien, K., Hoffman, R., 1990. Parvovirus B19-induced perturbation of human megakaryocytopoiesis in vitro. Blood 76, 1997–2004.

St Amand, J., Beard, C., Humphries, K., Astell, C.R., 1991. Analysis of splice junctions and in vitro and in vivo translation potential of the small, abundant B19 parvovirus RNAs. Virology 183, 133–142.

Yoto, Y., Qiu, J., Pintel, D.J., 2006. Identification and characterization of two internal cleavage and polyadenylation sites of parvovirus B19 RNA. J. Virol. 80, 1604–1609.

Young, N.S., Brown, K.E., 2004. Parvovirus B19. N. Engl. J. Med. 350, 586–597.

Zhi, N., Mills, I.P., Lu, J., Wong, S., Filippone, C., Brown, K.E., 2006. Molecular and functional analyses of a human parvovirus B19 infectious clone demonstrates essential roles for NS1, VP1, and the 11-kilodalton protein in virus replication and infectivity. J. Virol. 80, 5941–5950.